Coherent Control of Nitrogen-Vacancy Center Spins in Silicon Carbide at Room Temperature

Jun-Feng Wang,[1,2] Fei-Fei Yan,[1,2] Qiang Li,[1,2] Zheng-Hao Liu,[1,2] He Liu,[1,2] Guo-Ping Guo,[1,2] Li-Ping Guo,[3] Xiong Zhou,[3] Jin-Ming Cui,[1,2] Jian Wang,[1,2] Zong-Quan Zhou,[1,2] Xiao-Ye Xu,[1,2] Jin-Shi Xu,[1,2,*] Chuan-Feng Li,[1,2,†] and Guang-Can Guo[1,2]

[1]*CAS Key Laboratory of Quantum Information, University of Science and Technology of China, Hefei, Anhui 230026, People's Republic of China*

[2]*CAS Center for Excellence in Quantum Information and Quantum Physics, University of Science and Technology of China, Hefei, Anhui 230026, People's Republic of China*

[3]*Accelerator Laboratory, School of Physics and Technology, Wuhan University, Wuhan, Hubei 430072, People's Republic of China*

(Received 23 September 2019; accepted 27 April 2020; published 1 June 2020)

Solid-state color centers with manipulatable spin qubits and telecom-ranged fluorescence are ideal platforms for quantum communications and distributed quantum computations. In this work, we coherently control the nitrogen-vacancy (NV) center spins in silicon carbide at room temperature, in which telecom-wavelength emission is detected. We increase the NV concentration sixfold through optimization of implantation conditions. Hence, coherent control of NV center spins is achieved at room temperature, and the coherence time T_2 can be reached to around 17.1 μs. Furthermore, an investigation of fluorescence properties of single NV centers shows that they are room-temperature photostable single-photon sources at telecom range. Taking advantage of technologically mature materials, the experiment demonstrates that the NV centers in silicon carbide are promising platforms for large-scale integrated quantum photonics and long-distance quantum networks.

DOI: 10.1103/PhysRevLett.124.223601

The identification and coherent control of novel spin defects are important for extending the scope of solid-state quantum information science [1–3]. Optically active defect spins in solid-state systems have been widely used in quantum photonics, quantum communications, quantum computation, and quantum metrology [1–22]. Nitrogen-vacancy (NV) centers in diamond have become leading candidates due to their excellent properties, including photostability and long spin coherence times even at room temperature [4,5]. However, the drawbacks of visible-wavelength emission and the lack of a mature nanofabrication method for diamond limit their application to long-distance quantum communications and wafer-scale quantum technology [1–6]. To overcome these drawbacks, in recent years, defects in silicon carbide (SiC) have been developed as promising platforms for quantum information science [6–22].

SiC has been widely used in power electronic devices and has commercially available inch-scale growth and matured nanofabrication protocols [6–13]. Several bright (about Mcps) visible and telecom-range single-photon emitters have been found in different polytypes of SiC, which can be used for quantum photonics and quantum communications [7–10]. Moreover, as with NV centers in diamond, there are also optically active spin defects: silicon vacancy and divacancy defects in SiC, which can be polarized by laser and controlled by microwave [6,11–22]. These two kinds of defects have realized the single spin manipulation with long coherence times (about 1 ms) [11–16], high-fidelity near-infrared spin-to-photon interface [16,17], and high-sensitivity quantum metrologies for magnetic fields [18], electric fields [19], local strain fields [20], and temperature [21,22], etc. However, their emission spectra are only in the near infrared [6,11–16]. The efficient generation and coherent control of optically active spin defects with telecom-range emissions in SiC are still great challenges.

Most recently, NV centers in 4H-SiC and 3C-SiC have been demonstrated to be electron paramagnetic defects with emission at telecom wavelengths [23–30]. The $N_C V_{\mathrm{Si}}$ center in SiC consists of a nitrogen impurity substituting a carbon atom (N_C) and a silicon vacancy (V_{Si}) adjacent to it [23–30]. However, most previous experiments have focused on the properties of low-temperature (LT) photoluminescence (PL) spectra and electron paramagnetic resonance (EPR) of the NV centers [23–30]. Little is known about the optically-detected-magnetic-resonance (ODMR) spectrum and spin coherence property. Moreover, the scalable generation of single NV centers in SiC, which is vital for constructing on-chip quantum processors [6,11–17], has yet to be reported.

In this work, we realize coherent control of the NV center spins at room temperature and scalable generation

of the single NV centers in 4H-SiC. By optimizing the implanted conditions, the concentration of NV centers ensemble increases by about 6 times. The PL spectra of NV centers show that the wavelengths are in the telecom range. We then implement the ODMR measurement and realize coherent control of the NV center ensemble spins at room temperature with a coherence time T_2 of around 17.1 μs. Moreover, we find that the dephasing time T_2^* decreases as the nitrogen implanted dose increases from 1×10^{13} to 1×10^{16} cm^{-2}. Finally, we present the implanted single NV center and characterize the fluorescence property. Our experiments pave the way for using the NV centers in SiC for quantum photonics and quantum information processing.

In the experiment, a bulk high-purity 4H-SiC epitaxy layer sample is used [31,32]. To generate the shallow NV centers [60 nm, stopping and range of ions in matter (SRIM)] in 4H-SiC, 30 keV nitrogen ions are implanted [32]. The experiments are performed in a homebuilt confocal setup. A 1030 nm laser is used to excite the NV centers, since this pumping wavelength has a better exciting effect for NV centers and reduces the emission from the divacancy defects at the same time [24,27]. For the room-temperature confocal setup, an oil objective with 1.3 N.A. is used to excite the NV centers. The fluorescence is collected by a multimode fiber to a photoreceiver (Femto, OE-200-IN1) after a 1150 nm long pass (LP) filter for the spin control experiment of the NV center ensemble [21]. The spin signal is detected by lock-in methods [6,21,32]. To investigate the single NV defect, the fluorescence is collected by a single-mode fiber to a superconducting single-photon detector (Scontel) [22]. A Montana cryostation combined with a confocal setup is used for the low-temperature experiment [21,32].

Since the divacancies are intrinsic vacancy-related defects, it is inevitable that a few will be generated during the nitrogen implantation process [24,27]. Moreover, the PL and ODMR spectra of the NV centers in 4H-SiC are very close to that of the divacancy defects. In order to efficient fabricate single NV centers, it is critical to optimize the implanted conditions to efficiently generate the NV centers. In the experiment, the samples implanted with nitrogen ions with an influence of 1×10^{14} cm^{-2} are annealed at different temperatures for the same time (1 h). To measure the whole PL spectra of the sample, a 980 nm laser was used in the PL experiments. Figure 1(a) shows the low-temperature (20 K) PL spectra of the implanted samples at different annealing temperatures with a 1000 nm LP filter. The results show that the PL intensities of the zero phonon lines (ZPLs) of NV centers obviously increase as the annealing temperature increases from 800 °C to 1050 °C, while the PL intensities of the divacancy defects decrease at the same time, as shown in Supplemental Material [Fig. S1(b)] [33]. The corresponding scanning images of 10×10 μm^2 areas using the 1150 nm LP filter

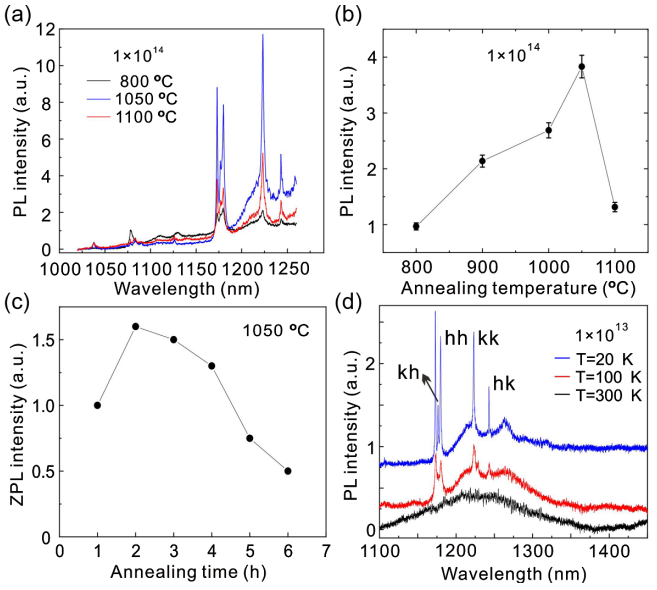

FIG. 1. (a) The LT-PL spectra of the NV centers and divacancy defects as a function of the annealing temperature. (b) The mean counts of the scanning images (10×10 μm^2) as a function of the annealing temperature with a pump laser power of 1 mW. (c) The NV center ZPL intensity as a function of the annealing time at 1050 °C. (d) The PL spectra of NV centers as the sample temperature increases from 20 to 300 K.

with a laser power of 1 mW are also investigated [33]. The mean counts of the scanning images (10×10 μm^2) are presented in Fig. 1(b). These counts increase by around 4 times as the annealing temperature increases from 800 °C to 1050 °C; then they decrease to about 1.3 times their original value at 1100 °C, which is similar to the previous deep-depth NV center implantation results [30]. Furthermore, as presented in Fig. 1(c), the optimal ZPL intensity for an annealing time of 2 h is 1.6 times larger than that for 1 h. Thus, the NV center concentration increases sixfold through optimization of the implantation conditions.

In addition, we also study the PL spectra of the sample (1×10^{13} cm^{-2}) as a function of the sample temperature increasing from 20 to 300 K [Fig. 1(d)]. We can see that the ZPL peaks of the NV centers decrease as the sample temperature increases, and they can still be observed when the temperature increases to 150 K [33]. At room temperature, the PL spectra range from 1100 to about 1420 nm, which covers the O-band and E-band telecom range for around 45%.

The electronic ground state of the negative nitrogen-vacancy (NV^-) center in 4H-SiC is a spin-1 state [23–29]. There are two types of bond directions for NV centers. One is c-axis defects (hh and kk, $C_{3\nu}$ symmetry), and another is basal defects (hk and kh, C_{1h} symmetry) [28]. The spin Hamiltonian is

$$H = D[S_z^2 - S(S+1)/3] + E(S_x^2 - S_y^2) + g\mu_B B S_z, \qquad (1)$$

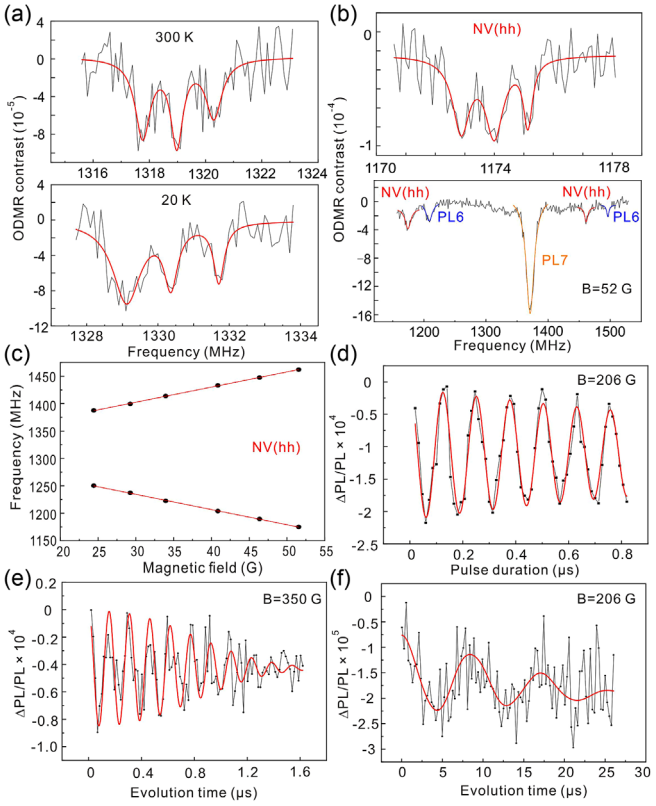

FIG. 2. (a) The ODMR measurement of the NV center (hh) ensemble at low (bottom, 20 K) and room (top, 300 K) temperature and zero magnetic field. The red lines are the fitting using the Lorentzian function. (b) The bottom shows the ODMR measurement of the NV center ensemble at room temperature and a magnetic field of 52 G. PL6 and PL7 are divacancy defects in 4H-SiC. The three peaks in the top part correspond to the nitrogen hyperfine coupling. (c) The ODMR resonant frequencies of the NV center ensemble as a function of the axial magnetic field. (d) The spin Rabi oscillation between $|0\rangle$ and $|-1\rangle$ states for the c-axis NV centers (hh) at room temperature. (e) The free induction decay of the NV center spins at room temperature. The red line is the fits of the data using the decayed sinuous function [33]. (f) Hahn echo measurement of the NV center ensemble.

where D and E are the axially symmetric and anisotropic components of the zero- field-splitting (ZFS) parameter, respectively, $g = 2$ is the electron g factor, μ_B is the Bohr magneton, and B is the applied axial static magnetic field. Moreover, they also have ^{14}N nuclear ($I = 1$) hyperfine interactions, which is around 1.2 MHz.

In the experiment, we focus only on the NV center (hh). First, ODMR measurements of the NV center (hh) ensemble (1×10^{14} cm^{-2} sample) with low laser and microwave power are performed at 20 K [bottom, Fig. 2(a)] and room temperature 300 K [top, Fig. 2(a)], respectively. The obvious three splittings at 1.3 MHz under both temperatures are due to the nitrogen nuclear hyperfine coupling. The low-temperature ZFS value is 1330.4 ± 0.1 MHz, and the hyperfine coupling A is around 1.3 MHz, which is the same as previous EPR reports of the NV center (hh) [28]. In addition, the room-temperature ZFS is around 1319.0 ± 0.1 MHz, which is 11.4 MHz smaller than the LT value. To further identify the bond direction of the observed defect spins, the magnetic-field-dependent ODMR measurement is also performed. The bottom part in Fig. 2(b) shows the ODMR measurement at 52 G, and the upper part shows the corresponding nitrogen hyperfine coupling. PL6 and PL7 are divacancy defects in 4H-SiC [11]. The summary of the two branch resonant frequencies as a function of the magnetic field is shown in Fig. 2(c). The red lines are the linear fitting to the data with slopes of 2.8 MHz/G. The corresponding ZFS value is around 1318.5 MHz, which is consistent with the directly measured value. These results demonstrate that the investigated spin is the c-axis NV center (hh). We further perform the angle-resolved hyperfine measurements by changing the angle of the external magnetic field. The results are displayed in Supplemental Material [33] and are consistent with the results shown here.

Coherent control of the spin state at room temperature is the cornerstone of NV center applications in quantum information processing [6,11–14]. Thus, we measure the Rabi oscillation of the NV center ensemble using a resonant microwave frequency of 742.3 MHz between $|0\rangle$ and $|-1\rangle$ states transition at 206 G using the standard pulse sequences [6,21,33]. The corresponding coherent Rabi oscillation of the NV centers at room temperature is shown in Fig. 2(d). Inferred from the fit, the Rabi frequency is about 7.9 MHz. The obvious oscillation signals demonstrate the coherent control of the NV center spins at room temperature [6,11,12,14]. The spin coherence properties of the NV centers in SiC are important for quantum computation and high-sensitivity quantum sensing [6,11,15,18–22,35,36]. Since an increase of the magnetic field could make the Ramsey fringe appear more clearly [37], we measure the free induction decay of the NV centers at room temperature with a magnetic field of around 350 G. The Ramsey fringe is shown in Fig. 2(e). The inferred dephasing time T_2^* is 1.0 ± 0.1 μs [33], which is comparable to the silicon vacancy [38] and divacancy [14,16] in SiC. As presented in Fig. 2(f), the Hahn echo is also investigated, and the periodic modulations of its envelope are due to the ^{29}Si and ^{13}C nuclear spin bath. The inferred coherence time $T_2 = 17.1 \pm 4.0$ μs [33], which is comparable to the previous room-temperature divacancy defects ensemble and silicon vacancy ensemble results [6,39].

We further investigate the influence of the implanted doses on the coherence properties [11,35]. The LT-PL spectra of NV centers for different doses are shown in Fig. 3(a), which both have obvious NV center ZPLs. Figure 3(b) shows mean counts of the NV centers as a function of the dose. The counts increase with the dose from 1×10^{12} to 1×10^{15} cm^{-2} while slightly decreasing when the dose increases to 1×10^{16} cm^{-2}. The saturation of the counts may be due to the nitrogen ion implanted damage to crystal lattices, leading to amorphization of

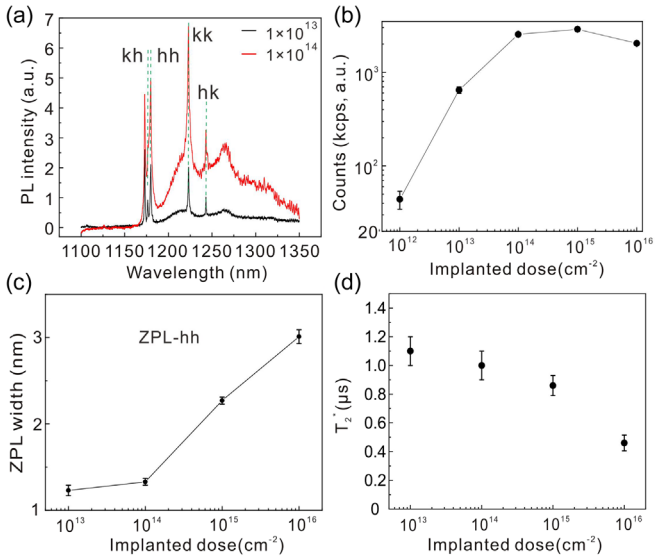

FIG. 3. (a) The LT (20 K) PL spectra of the NV center ensemble with different implanted doses. (b) The mean counts of the NV centers on samples with different implanted doses. (c) The widths of ZPL of the NV center (*hh*) as a function of the implanted dose. (d) Comparison of the dephasing time T_2^* for samples with four different implanted doses.

the SiC [32]. We also study the changes of the width of NV center (*hh*) ZPL as the dose increases. As shown in Fig. 3(c), the ZPL width slowly increases from 1.2 to 1.3 nm as the dose increases from 1×10^{13} to 1×10^{14} cm^{-2} before rapidly increasing to 3.0 nm as the dose increases to 1×10^{16} cm^{-2}. Moreover, we compare the free induction decay of the sample with the different implanted dose. The NV center ensemble dephasing time T_2^* as a function of the implanted dose is presented in Fig. 3(d). The T_2^* decreases slightly as the dose increases from 1×10^{13} to 1×10^{15} cm^{-2}, and then it quickly decreases to 0.45 μs as the dose increases to 1×10^{16} cm^{-2}. The decrease of the T_2^* may be due to the increase of the defect densities and the damage to the lattice of the SiC [11].

Generating single NV centers in SiC is vital for various quantum technologies, including quantum photonics, quantum networks, and nanoscale quantum sensing [5,12–14, 16,17,31,32,40,41]. In our experiment, a 200-nm-thick polymethyl methacrylate (PMMA) layer is deposited on the SiC surface. Then, 70 ± 10 nm diameter nanoaperture arrays (2×2 μm^2) are generated using electron-beam lithography technology [31,32]. 30 keV nitrogen ions with a dose of 2.5×10^{11} cm^{-2} are implanted through the nanoapertures to generate a single NV center array in 4H-SiC.

We then characterize the fluorescence properties of the generated single NV centers. A representative 20×20 μm^2 confocal image of the single-defect arrays is displayed in Fig. 4(a). To identify the number of NV centers, we perform the Hanbury-Brown and Twiss (HBT) measurement and obtain the corresponding second-order photon

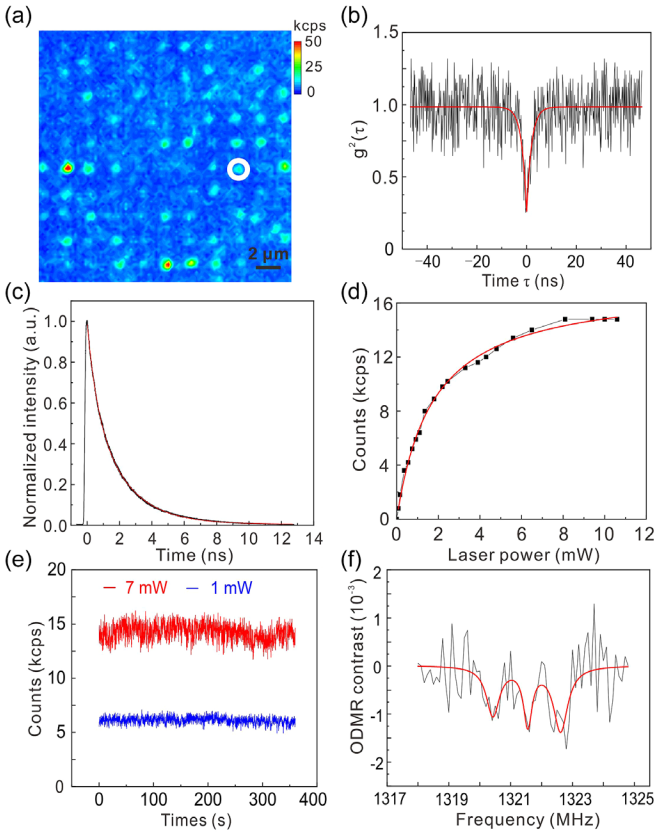

FIG. 4. (a) A confocal scan image (20×20 μm^2) of the single NV center arrays in 4H-SiC with a laser power of 4 mW. The circled point is the investigated single NV center. The scale bar is 2 μm. (b) The correlation function measurement of the circled single NV center in (a). (c) The lifetime of the NV center ensemble at room temperature. (d) The counts of the single NV centers as a function of the laser power. (e) The photostability of the single NV center at two different pump laser powers with the time bin set to 100 ms. (f) The ODMR measurement of a single NV center.

correlation function. Figure 4(b) presents the result for the circled defects in Fig. 4(a). Then we fit $g^2(\tau)$ using the function $g^2(\tau) = 1 - a^* \exp(-|\tau|/\tau_1) + b^* \exp(-|\tau|/\tau_2)$, where a and b are fitting parameters and τ_1 and τ_2 are related to the excited and metastable state lifetimes, respectively. The obtained $g^2(0)$ is around 0.25, which demonstrates that it is a single defect [33]. Inferred from the fit, the τ_1 and τ_2 are about 2.4 and 450 ns, respectively. Moreover, we measure the fluorescence lifetime of the NV centers in the same sample using a 1040 nm femtosecond pulse laser at both room temperature and a low temperature. Figure 4(c) shows the lifetime of the NV center ensemble at room temperature. The red line is the fit of the data using a double-exponential decay function. The fluorescence lifetime is about 2.1 ± 0.1 ns, which is almost the same as the short excited state lifetimes τ_1 [42,43]. The lifetime is much smaller than that of the divacancy in 4H-SiC [14,16,20,44].

The saturation curve of a single NV center is shown in Fig. 4(d). The red line is the fitting using the power dependence model $I(P) = I_s/(1 + P_0/P)$, where I_s is the maximal emission counts and P_0 is the saturation power. The fit indicates that I_s is around 17.4 ± 0.2 kcps and the saturation power P_0 is around 1.7 ± 0.1 mW, respectively. The saturation count is comparable with silicon vacancy and divacancy in 4H-SiC [12,16]. The low count rate might come from trapping in other dark states [31]. Figure 4(e) exhibits the time trace of counts of the single NV centers for about 6 min with a 100 ms time bin for two different pump laser powers. The stable fluorescence emission demonstrates that the NV center is a stable infrared-wavelength single-photon source at room temperature. Furthermore, we also measured the single NV center ODMR [Fig. 4(f)]. Inferred from the fitting, the ZFS is 1321.5 MHz, and the little difference from the ensemble value may due to the different residual strains in different samples [31]. In addition, the nitrogen hyperfine coupling is around 1.1 MHz, which is consistent with previous EPR reports [28].

In conclusion, we coherently control the NV center spins and characterize the fluorescence and ODMR properties of a single NV centers in 4H-SiC at room temperature. Through optimizing the annealing condition, the concentration of the NV centers increases about 6 times. Furthermore, we coherently control the spin states of the NV centers (hh) ensemble at room temperature and obtain a coherence time T_2 of around 17.1 μs, which is comparable to that of the divacancy and silicon vacancy defects in SiC [6,39]. The dephasing time T_2^* is shown to decrease as the implanted dose increases. The single NV centers are demonstrated to be room-temperature photostable with a saturation count of around 17.4 kcps, which is comparable to divacancy [14,16] and silicon vacancy [12,13,31,32] in 4H-SiC. The experiment paves the way for using NV centers in technologically friendly SiC materials in quantum photonics, quantum information processing, and scalable quantum networks.

We thank Professor J. Wrachtrup for the helpful discussion. We also thank Yongxiang Zheng and Jun Hu for their help in the experiment. This work was supported by the National Key Research and Development Program of China (Grants No. 2016YFA0302700 and No. 2017YFA0304100), the National Natural Science Foundation of China (Grants No. 61725504, No. 61905233, No. 11975221, No. 11804330, No. 11821404, No. 11774335, and No. U19A2075), the Key Research Program of Frontier Sciences, Chinese Academy of Sciences (CAS) (Grant No. QYZDY-SSW-SLH003), Science Foundation of the CAS (No. ZDRW-XH-2019-1), Anhui Initiative in Quantum Information Technologies (AHY060300 and AHY020100), and the Fundamental Research Funds for the Central Universities (Grants No. WK2030380017 and No. WK2470000026).

*Corresponding author.
jsxu@ustc.edu.cn
†Corresponding author.
cfli@ustc.edu.cn

[1] J. R. Weber, W. F. Koehl, J. B. Varley, A. Janotti, B. B. Buckley, C. G. Van de Walle, and D. D. Awschalom, Proc. Natl Acad. Sci. U.S.A. **107**, 8513 (2010).
[2] D. D. Awschalom, R. Hanson, J. Wrachtrup, and B. B. Zhou, Nat. Photonics **12**, 516 (2018).
[3] M. Atatüre, D. Englund, N. Vamivakas, S.-Y. Lee, and J. Wrachtrup, Nat. Rev. Mater. **3**, 38 (2018).
[4] A. Gruber, A. Dräbenstedt, C. Tietz, L. Fleury, J. Wrachtrup, and C. von Borczyskowski, Science **276**, 2012 (1997).
[5] B. Hensen, H. Bernien, A. E. Dréau, A. Reiserer, N. Kalb, M. S. Blok, J. Ruitenberg, R. F. L. Vermeulen, R. N. Schouten, C. Abellán, W. Amaya, V. Pruneri, M. W. Mitchell, M. Markham, D. J. Twitchen, D. Elkouss, S. Wehner, T. H. Taminiau, and R. Hanson, Nature (London) **526**, 682 (2015).
[6] W. F. Koehl, B. B. Buckley, F. J. Heremans, G. Calusine, and D. D. Awschalom, Nature (London) **479**, 84 (2011).
[7] S. Castelletto, B. C. Johnson, V. Ivády, N. Stavrias, T. Umeda, A. Gali, and T. Ohshima, Nat. Mater. **13**, 151 (2014).
[8] A. Lohrmann, B. C. Johnson, J. C. McCallum, and S. Castelletto, Rep. Prog. Phys. **80**, 034502 (2017).
[9] J. F. Wang, Y. Zhou, Z. Y. Wang, A. Rasmita, J. Q. Yang, X. J. Li, H. J. von Bardeleben, and W. B. Gao, Nat. Commun. **9**, 4106 (2018).
[10] Q. Li, J. Y. Zhou, Z. H. Liu, J. S. Xu, C. F. Li, and G. C. Guo, J. Semicond. **40**, 072902 (2019).
[11] A. L. Falk, B. B. Buckley, G. Calusine, W. F. Koehl, V. V. Dobrovitski, A. Politi, C. A. Zorman, P. X.-L. Feng, and D. D. Awschalom, Nat. Commun. **4**, 1819 (2013).
[12] M. Widmann, S.-Y. Lee, T. Rendler, N. T. Son, H. Fedder, S. Paik, L.-P. Yang, N. Zhao, S. Yang, I. Booker, A. Denisenko, M. Jamali, S. A. Momenzadeh, I. Gerhardt, T. Ohshima, A. Gali, E. Janzén, and J. Wrachtrup, Nat. Mater. **14**, 164 (2015).
[13] F. Fuchs, B. Stender, M. Trupke, D. Simin, J. Pflaum, V. Dyakonov, and G. V. Astakhov, Nat. Commun. **6**, 7578 (2015).
[14] D. J. Christle, A. L. Falk, P. Andrich, P. V. Klimov, J. Ul Hassan, N. T. Son, E. Janzén, T. Ohshima, and D. D. Awschalom, Nat. Mater. **14**, 160 (2015).
[15] P. V. Klimov, A. L. Falk, D. J. Christle, V. V. Dobrovitski, and D. D. Awschalom, Sci. Adv. **1**, e1501015 (2015).
[16] D. J. Christle, P. V. Klimov, F. Charles, K. Szász, V. Ivády, V. Jokubavicius, J. Ul Hassan, M. Syväjärvi, W. F. Koehl, and T. Ohshima, E. Janzén, Á. Gali, and D. D. Awschalom, Phys. Rev. X **7**, 021046 (2017).
[17] R. Nagy, M. Niethammer, M. Widmann, Y.-C. Chen, P. Udvarhelyi, C. Bonato, J. Ul Hassan, R. Karhu, I. G. Ivanov, N. T. Son, J. R. Maze, T. Ohshima, Ö. O. Soykal, Á. Gali, S.-Y. Lee, F. Kaiser, and J. Wrachtrup, Nat. Commun. **10**, 1954 (2019).
[18] D. Simin, V. A. Soltamov, A. V. Poshakinskiy, A. N. Anisimov, R. A. Babunts, D. O. Tolmachev, E. N. Mokhov, M. Trupke, S. A. Tarasenko, A. Sperlich, P. G. Baranov,

V. Dyakonov, and G. V. Astakhov, Phys. Rev. X **6**, 031014 (2016).
[19] G. Wolfowicz, S. J. Whiteley, and D. D. Awschalom, Proc. Natl. Acad. Sci. U.S.A. **115**, 7879 (2018).
[20] A. L. Falk, P. V. Klimov, B. B. Buckley, V. Ivády, I. A. Abrikosov, G. Calusine, W. F. Koehl, Á. Gali, and D. D. Awschalom, Phys. Rev. Lett. **112**, 187601 (2014).
[21] Y. Zhou, J. F. Wang, X. M. Zhang, K. Li, J. M. Cai, and W. B. Gao, Phys. Rev. Applied **8**, 044015 (2017).
[22] F. F. Yan, J. F. Wang, Q. Li, Z. D. Cheng, J. M. Cui, W. Z. Liu, J. S. Xu, C. F. Li, and G. C. Guo, Phys. Rev. Applied **10**, 044042 (2018).
[23] H. J. Von. Bardeleben, J. L. Cantin, E. Rauls, and U. Gerstmann, Phys. Rev. B **92**, 064104 (2015).
[24] S. A. Zargaleh, B. Eble, S. Hameau, J.-L. Cantin, L. Legrand, M. Bernard, F. Margaillan, J.-S. Lauret, J.-F. Roch, H. J. von Bardeleben, E. Rauls, U. Gerstmann, and F. Treussart, Phys. Rev. B **94**, 060102(R) (2016).
[25] H. J. Von Bardeleben, J. L. Cantin, A. Csóré, A. Gali, E. Rauls, and U. Gerstmann, Phys. Rev. B **94**, 121202(R) (2016).
[26] A. Csóré, H. J. Von Bardeleben, J. L. Cantin, and A. Gali, Phys. Rev. B **96**, 085204 (2017).
[27] B. Magnusson, N. T. Son, A. Csóré, A. Gällström, T. Ohshima, A. Gali, and I. G. Ivanov, Phys. Rev. B **98**, 195202 (2018).
[28] S. A. Zargaleh, H. J. von Bardeleben, J. L. Cantin, U. Gerstmann, S. Hameau, B. Eblé, and W. B. Gao, Phys. Rev. B **98**, 214113 (2018).
[29] S. A. Zargaleh, S. Hameau, B. Eble, F. Margaillan, H. J. von Bardeleben, J. L. Cantin, and W. B. Gao, Phys. Rev. B **98**, 165203 (2018).
[30] S. I. Sato, T. Narahara, Y. Abe, Y. Hijikata, T. Umeda, and T. Ohshima, J. Appl. Phys. **126**, 083105 (2019).
[31] J. F. Wang, Y. Zhou, X. M. Zhang, F. C. Liu, Y. Li, K. Li, Z. Liu, G. Z. Wang, and W. B. Gao, Phys. Rev. Applied **7**, 064021 (2017).
[32] J. F. Wang, Q. Li, F. F. Yan, H. Liu, G. P. Guo, W. P. Zhang, X. Zhou, L. P. Guo, Z. H. Lin, J. M. Cui, X. Y. Xu, J. S. Xu, C. F. Li, and G. C. Guo, ACS Photonics **6**, 1736 (2019).
[33] See Supplemental Material at http://link.aps.org/supplemental/10.1103/PhysRevLett.124.223601 for the PL spectrum, PL images of the NV centers, pulse sequences for coherent control of the NV centers, statistics of the implanted NV center array, energy-level model for the ODMR contrast, ODMR spectrum as a function of the magnetic field angle, and ODMR of the single NV center at a *c*-axis magnetic field, which includes Ref. [34].
[34] P. G. Baranov, A. P. Bundakova, A. A. Soltamov, S. B. Orlinskii, I. V. Borovykh, R. Zondervan, R. Verberk, and J. Schmidt, Phys. Rev. B **83**, 125203 (2011).
[35] H. Seo, A. L. Falk, P. V. Klimov, K. C. Miao, G. Galli, and D. D. Awschalom, Nat. Commun. **7**, 12935 (2016).
[36] J.-P. Tetienne, R. W. de Gille, D. A. Broadway, T. Teraji, S. E. Lillie, J. M. McCoey, N. Dontschuk, L. T. Hall, A. Stacey, D. A. Simpson, and L. C. L. Hollenberg, Phys. Rev. B **97**, 085402 (2018).
[37] J. R. Maze, A. Dréau, V. Waselowski, H. Duarte, J.-F. Roch, and V. Jacques, New J. Phys. **14**, 103041 (2012).
[38] R. Nagy, M. Widmann, M. Niethammer, D. B. R. Dasari, I. Gerhardt, O. O. Soykal, M. Radulaski, T. Ohshima, J. Vučković, N. T. Son, I. G. Ivanov, S. E. Economou, C. Bonato, S.-Y. Lee, and J. Wrachtrup, Phys. Rev. Applied **9**, 034022 (2018).
[39] D. Simin, H. Kraus, A. Sperlich, T. Ohshima, G. V. Astakhov, and V. Dyakonov, Phys. Rev. B **95**, 161201(R) (2017).
[40] T. Schröder, M. E. Trusheim, M. Walsh, L. Li, J. Zheng, M. Schukraft, A. Sipahigil, R. E. Evans, D. D. Sukachev, C. T. Nguyen, J. L. Pacheco, R. M. Camacho, E. S. Bielejec, M. D. Lukin, and D. Englund, Nat. Commun. **8**, 15376 (2017).
[41] M. Radulaski, M. Widmann, M. Niethammer, J. L. Zhang, S. Y. Lee, T. Rendler, K. G. Lagoudakis, N. T. Son, E. Janzen, T. Ohshima, J. Wrachtrup, and J. Vučković, Nano Lett. **17**, 1782 (2017).
[42] A. M. Berhane, K.-Y. Jeong, C. Bradac, M. Walsh, D. Englund, M. Toth, and I. Aharonovich, Phys. Rev. B **97**, 165202 (2018).
[43] G. Wolfowicz, C. P. Anderson, B. Diler, O. G. Poluektov, F. J. Heremans, and D. D. Awschalom, arXiv:1908.09817.
[44] C. P. Anderson, A. Bourassa, K. C. Miao, G. Wolfowicz, P. J. Mintun, A. L. Crook, H. Abe, J. Ul Hassan, N. T. Son, T. Ohshima, and D. D. Awschalom, Science **366**, 1225 (2019).